Renewable Energy and Power Quality Journal
https://repqj.com/index.php/repqj/index
RE&PQJ, Vol. 24, No. 1, 2026

Energy Management for Ground-Generation Airborne Wind Energy Systems

Pablo Flores-Martín[1,2], Carolina Nicolás-Martín[1], Osmany R. Pérez-Aballe[3], Jorge González-García[4], and David Santos-Martín[1]

[1]Department of Electrical Engineering, Universidad Carlos III de Madrid, Avenida de la Universidad 30, 28911 Leganés (Madrid), Spain
[2]CT Ingenieros A.A.I. S.L., Avenida Leonardo Da Vinci 22, 28050 Getafe (Madrid), Spain
[3]Department of Electrical Engineering, University of Moa, Moa, Holguín, Cuba
[4]Department of Aerospace Engineering, Universidad Carlos III de Madrid, Avenida de la Universidad 30, 28911 Leganés (Madrid), Spain

Abstract

Airborne Wind Energy Systems (AWES) offer a promising alternative to conventional wind turbines, enabling access to high-altitude winds with greater energy yield and reduced infrastructure costs. However, integrating AWES into power grids poses challenges due to their cyclic power generation profile. This research develops an Energy Management System (EMS) to optimize power distribution, load balancing, and energy storage in AWES-based microgrids.

The proposed EMS employs a state-based control approach implemented in MATLAB/Simulink's Stateflow environment, dynamically adjusting power flows to stabilize the grid. A comprehensive simulation framework in Simulink models AWES interactions with battery storage and grid loads, allowing real-time validation of operational scenarios. Results demonstrate the EMS's effectiveness in mitigating power fluctuations, enhancing grid resilience, and maximizing renewable energy utilization. This study contributes to the broader integration of AWES into decentralized energy systems, supporting the transition toward reliable and sustainable energy solutions.

Keywords: Airborne Wind Energy, Energy Management System, Microgrid, Stateflow, Renewable Energy Integration.

1. Introduction

Airborne Wind Energy Systems (AWES) have gained considerable attention in recent years as a promising technology to harvest high-altitude winds at relatively lower installation and maintenance costs compared to conventional wind turbines [1],[2]. Conventional wind turbines are limited in height due to structural, economic, and logistical constraints. Building taller towers becomes increasingly expensive and complex, while the added power output does not justify the increased material and engineering challenges [3].

AWES overcome these challenges by using tethered aircraft that operate at altitudes of 300–600 meters [4], where wind speeds are significantly stronger and more consistent [5],[6]. Much like the outer edge of a conventional turbine blade benefits from higher apparent wind velocity, a kite in an AWES acts as an extended, fast-moving blade tip [7]. By continuously flying crosswind maneuvers, typically in figure-eight patterns, the kite experiences intensified relative wind speeds, boosting lift and power generation without the need for a full tower structure [8]-[10]. This design harnesses the most efficient section of a typical turbine blade but in a considerably lighter, more flexible format [11], making it feasible to develop wind farms in regions with insufficient low-level wind speeds for traditional turbines. Moreover, by reaching higher altitudes, AWES achieve a greater capacity factor, capitalizing on more stable and powerful winds [6].

Airborne Wind Energy Systems can be broadly categorized into fly-generation and ground-generation designs. Fly-generation AWES place the power generator on the airborne platform, whereas ground-generation AWES rely on a tethered wing pulling a generator on the ground [2],[4] as illustrated in Figure 1.

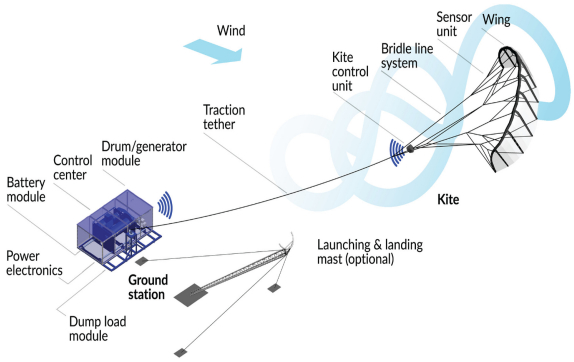

Figure 1: Components of a ground-generation AWES. Adapted from [12].

The latter, which is the focus of this study, operates in a cyclical manner by unwinding and rewinding a tether around a drum. During the "reel-out" phase, the wing

performs crosswind maneuvers that pull the tether under high tension, spinning a winch to generate electrical power. Once the tether reaches its maximum extension, the system transitions into the "reel-in" phase, during which the wing's drag is minimized and the tether is retracted with significantly lower energy expenditure [7],[13]. A conceptual illustration of this cycle is shown in Figure 2.

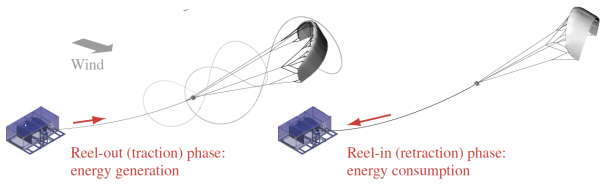

Figure 2: Working principle of the pumping cycle of a kite power system [13].

In ground-generation AWES, this cyclic behavior results in alternating periods of power generation (reel-out) and power consumption (reel-in). Furthermore, the mechanical dynamics of crosswind maneuvers—often figure-eight flight paths—introduce substantial fluctuations in the electrical output [10],[11], as illustrated in Figure 3. Consequently, advanced energy management strategies are critical for ensuring grid stability when integrating power from AWESs.

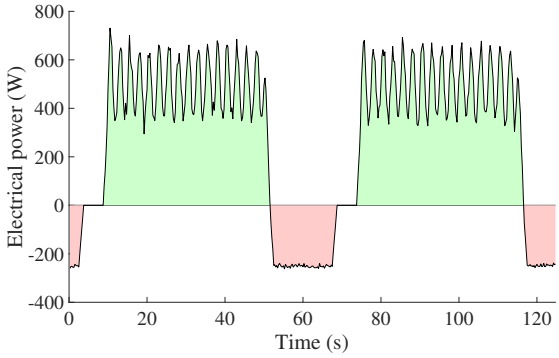

Figure 3: Conceptual electrical power profile over time in a ground-generation AWES. During the reel-out phase (green area), power output is positive with significant fluctuations, while in the reel-in phase (red area), it becomes negative and relatively steady.

Although power conversion systems are a necessary area of research for AWES, they remain relatively underexplored in the existing scientific literature. This is primarily due to the logical prioritization of research efforts and resources toward the development of the airborne component, its control mechanisms, and ensuring the mechanical feasibility of the technology. However, as AWES technology approaches the pre-commercial phase, research on power conversion systems tailored for these applications has become increasingly urgent.

Several studies, including [14]-[17], have investigated and proposed various electrical power conversion topologies for AWES, including the integration of Energy Storage System (ESS). Despite these contributions, a critical gap remains: none of these studies propose a dedicated Energy Management System (EMS) control strategy tailored to the specific dynamics of AWES power conversion.

This paper bridges this gap by presenting a novel EMS tailored for microgrids integrating an AWES unit. Implemented in MATLAB/Simulink's Stateflow environment, the proposed EMS dynamically optimizes power routing and storage utilization to ensure a stable electricity supply. This is particularly crucial in mitigating the fluctuations inherent in the cyclic reel-out/reel-in operation characteristic of ground-generation AWES.

The proposed control strategy is initially validated in a Software-in-the-loop (SiL) simulation that replicates the targeted microgrid architecture. Following this virtual testing, the EMS is deployed in a physical microgrid, where a realistic power cycle is injected to evaluate system performance under real operating conditions. Developing the simulation first mitigates the risk of controller malfunctions and establishes a scalable framework for various microgrid configurations.

This document presents the methodology, implementation, and results of the proposed EMS for a ground-generation AWES microgrid. In subsection 2.1, the microgrid hardware is introduced, highlighting its electrical topology and key components. Subsection 2.2 then outlines the EMS requirements and functionality, emphasizing the control logic that governs energy management. Next, subsection 2.3 explains how this logic is applied at the component level by detailing the control of each DC–DC converter. Finally, subsection 2.4 presents the SiL simulation and outlines the process of converting the EMS from MATLAB/Simulink's Stateflow environment into deployable PLC code.

Subsection 3.1 describes the state diagram that governs the EMS. Subsequently, subsection 3.2 presents the simulation outcomes, and subsection 3.3 summarizes the initial Hardware-in-the-loop (HiL) testing. Finally, section 4 offers a concise review of the key findings and proposes directions for future work.

2. Methodology

This section outlines the technical foundation of the proposed EMS and its integration into the ground-generation AWES microgrid. In particular, it details the hardware components in the microgrid testbed, describes the functional requirements that guide the EMS design, and explains how the control strategy is implemented at both the system and component levels.

2.1. Microgrid Hardware Description

Figure 4 shows the proposed electric topology for the microgrid. It employs a parallel structure with a common DC bus. Its key hardware elements include:

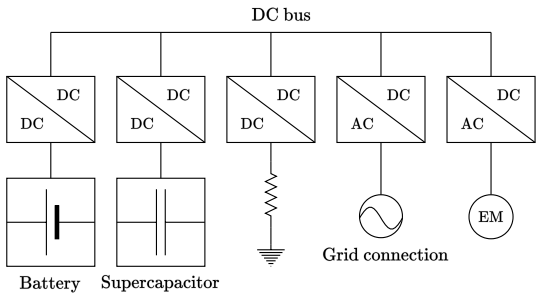

Figure 4: Proposed electric topology for AWES power conversion.

- **Electric Machine (EM) Connected to the AWES**: A DC-AC power converter enables precise control of the

electromagnetic torque in a three-phase electric generator connected to a drum, allowing the aircraft to generate optimal power while flying in figure-eight patterns. This results in an optimal, although dynamic, power profile fed into the microgrid, as illustrated in Figure 2.

- **Grid Connection**: The proposed microgrid supports both islanded and grid-connected operation through a DC-AC power converter, which ensures a stable power supply to the grid.
- **ESSs**: The DC storage system in the proposed microgrid relies on two complementary energy storage technologies, each serving a distinct purpose. A supercapacitor is employed for rapid energy exchanges, handling sudden power fluctuations and highly dynamic inrush currents. It responds almost instantly, ensuring smooth operation during transient events. A battery maintains a stable DC bus and stores excess energy for later use. Unlike the supercapacitor, it prioritizes long-term energy storage and steady power delivery rather than fast charging and discharging. By integrating both technologies, the system effectively balances the short-term high-power demands of the AWES power profile with overall energy stability and reliability.
- **Safety Components**: A braking resistor ensures safe operation by dissipating excess energy when needed, thereby preventing overvoltage conditions.
- **Bi-directional DC-DC Power Converters**: Every ESS element has a dedicated bidirectional DC-DC buck-boost converter for charging or discharging the storage elements by controlling both high- and low voltage side voltages and currents. Additionally, the braking resistor is also connected through its own dedicated DC-DC converter, allowing controlled energy dissipation when required.

Every component is instrumented with sensors and communication interfaces that transmit real-time operational data (e.g., voltages, currents, State of Charge (SoC) levels) to a Programmable Logic Controller (PLC).

2.2. EMS Requirements and Functionality

The proposed EMS aims to efficiently manage the energy generated by the kite in real time. By coordinating the charging and discharging of each ESS, it ensures bus voltage stability, maintains appropriate SoC levels across all ESSs, and sustains a continuous power flow to the grid. Specifically:

- During the **reel-out phase**, when the kite generates power, the supercapacitor absorbs transient power fluctuations, while in parallel, part of the generated power goes to the grid.
- During the **reel-in phase**, when the kite consumes power to retract the tether, the supercapacitor (having stored sufficient energy) discharges to meet both the retraction demand and the grid's requirements. This discharge frees up capacity in the supercapacitor, preparing it for the next cycle of power generation.

This behavior is illustrated in Figure 5, where the continuous line denotes the power generated by the kite and the dashed line represents the power delivered to the grid. During the reel-out phase, part of the generated power is fed directly into the grid (yellow area), while the supercapacitor absorbs transient fluctuations (gray area). During the reel-in phase, the supercapacitor discharges to supply power for tether retraction (blue area) and to maintain a stable flow to the grid (blue and yellow striped area). Ideally, the gray and both blue areas would be equal, meaning the supercapacitor absorbs and releases the same amount of energy each cycle and thus returns to its initial voltage.

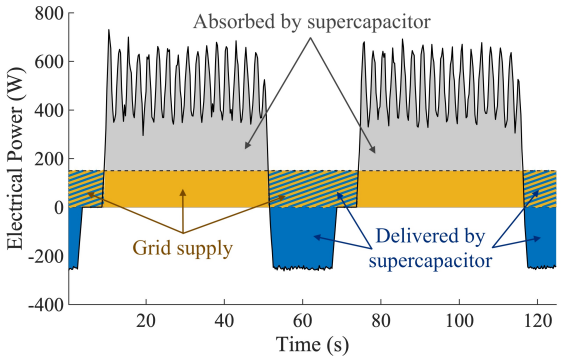

Figure 5: Conceptual representation of power flows among microgrid components during a reel-out and reel-in cycle.

In practice, however, the net energy is rarely zero, especially during islanded operation. If the net energy is positive, the supercapacitor finishes the cycle with a higher charge than it started with; if negative, it ends with a lower charge. Consequently, the battery must store or supply energy to keep the supercapacitor's charge within acceptable limits.

To determine the required energy, the EMS uses both predictive and feedback control. At the end of each cycle, the predictive component estimates the next cycle's net energy requirement, while the feedback component measures the supercapacitor's voltage and calculates the energy needed to restore it to its initial value. This approach keeps the supercapacitor's net energy exchange close to zero each cycle. The process proceeds as follows:

The net energy for the next cycle is:

$$E_{\text{net}}[n+1] = E_{\text{reel-out}}[n+1] - E_{\text{reel-in}}[n+1] - E_{\text{grid}}[n+1], \tag{1}$$

In this context, the subscript $[n+1]$ denotes values predicted by the EMS for the upcoming operation cycle. Accordingly, $E_{\text{reel-out}}[n+1]$ refers to the estimated energy production during the reel-out phase, $E_{\text{reel-in}}[n+1]$ to the estimated energy consumption during reel-in, and $E_{\text{grid}}[n+1]$ to the anticipated net energy delivered to the grid throughout the next full cycle.

Additionally, the difference in supercapacitor energy between the end of cycle n and its initial state is:

$$\begin{aligned} E_{\text{SC diff}}[n] &= E_{\text{SC}}[n] - E_{\text{SC}}[0], \\ &= \tfrac{1}{2}\, C\big(V_{\text{SC}}[n]^2 - V_{\text{SC}}[0]^2\big), \end{aligned} \tag{2}$$

where $E_{\text{SC}}[n]$ denotes the supercapacitor energy at the start of cycle n, and $E_{\text{SC}}[0]$ is its initial (or reference) energy. The parameter C is the supercapacitor's capacitance, $V_{\text{SC}}[n]$ is its voltage at the beginning of cycle n, and $V_{\text{SC}}[0]$ is the initial or reference voltage.

By combining Equations 1 and 2, the total energy that the battery must absorb or supply in the next cycle in order for the supercapacitor's net energy to be zero is:

$$E_{\text{bat}}[n+1] = E_{\text{net}}[n+1] + E_{\text{SC diff}}[n]. \tag{3}$$

However, it is not always necessary to keep the supercapacitor's net energy exchange strictly at zero every cycle. If the energy from Equation 3 is sufficiently small (in absolute value), the supercapacitor's end-of-cycle charge will not deviate significantly from its initial level, making it unnecessary to cycle the battery. Avoiding these small

charge–discharge operations prolongs battery life. Hence, the continuous power required from the battery in the next cycle is given by:

$$|E_{\text{bat}}|\,[n+1] \begin{cases} < E_{\min}, & P_{\text{bat}}[n+1] = 0, \\ \geq E_{\min}, & P_{\text{bat}}[n+1] = \frac{E_{\text{bat}}[n+1]}{T_{\text{cycle}}[n+1]}, \end{cases} \tag{4}$$

where $E_{\min}$ is the minimum required energy for the battery to be involved, $P_{\text{bat}}[n+1]$ is the continuous power needed form the battery over one cycle (positive during charging, negative during discharging), and $T_{\text{cycle}}[n+1]$ is the duration of the next complete cycle.

To replicate the supercapacitor behavior shown in Figure 5, while still allowing the battery to regulate the net energy balance, the instantaneous supercapacitor power (positive when absorbing, negative when releasing) is defined as:

$$P_{\text{SC}} = P_{\text{EM}} - P_{\text{grid}} - P_{\text{bat}}, \tag{5}$$

where P_{EM} is the power from the electric machine (positive when supplying, negative when consuming) and P_{grid} is the power delivered to the grid.

Additionally, the EMS monitors the battery's SoC and halts operation whenever critical thresholds are approached.

2.3. DC–DC Converters Control

To achieve the desired ESS behavior described in subsection 2.2 while maintaining system stability, each converter operates in the following control modes:

- **Battery DC–DC Converter:** This converter maintains the bus voltage within the range of 1 to 1.06 per unit (p.u.). While the voltage remains within these bounds, the converter stays idle, minimizing power flow through the battery. When the voltage deviates from this range, the converter injects or absorbs energy to bring it back within limits. As a result, power delivery from the battery is not continuous, but occurs in bursts of discrete 1 p.u. current spikes. The internal bus capacitance slows the voltage response, spacing out these spikes and producing a characteristic sawtooth pattern in the bus voltage. This control strategy enhances converter efficiency and allows the battery to remain idle for extended periods.

  Since the converter operates strictly in voltage-control mode (i.e., it cannot regulate current directly), the only way to initiate the required energy exchange is for the supercapacitor to deliberately shift the bus voltage by adjusting the power it absorbs or delivers, as defined by the P_{bat} term in Equation 5. This controlled variation in bus voltage triggers the battery to deliver or absorb the energy specified in Equation 3 over one complete cycle, ensuring the proper energy exchange.

- **Supercapacitor DC–DC Converter:** This converter regulates the internal (low voltage side) supercapacitor voltage and imposes a dynamic current limit on the same side.

  To ensure the supercapacitor absorbs or delivers the power specified in Equation 5, both the voltage reference and the current limit must be configured accordingly. The voltage reference is set as follows:

$$P_{\text{SC}} \begin{cases} < 0, & V_{\text{SC ref}} = V_{\text{SC min}}, \\ \geq 0, & V_{\text{SC ref}} = V_{\text{SC max}}, \end{cases} \tag{6}$$

  where $V_{\text{SC ref}}$ is the reference voltage sent to the supercapacitor converter, $V_{\text{SC min}}$ is the minimum allowable voltage, and $V_{\text{SC max}}$ is the maximum allowable voltage.

  The corresponding low voltage side current limit is defined as:

$$I_{\text{SC lim}} = \frac{|P_{\text{SC}}|}{V_{\text{SC}}}, \tag{7}$$

  ensuring that the supercapacitor follows the target current magnitude.

  This configuration enables precise control over the supercapacitor's charge and discharge behavior, while guaranteeing that its voltage remains within the permissible range at all times.

- **Safety Control Strategy**: To ensure safe operation, a dedicated control strategy manages overvoltage conditions. A dissipation control system remains inactive under normal conditions but activates when the bus voltage exceeds a predefined threshold. Using a droop current control strategy, it gradually increases current draw to dissipate excess energy and regulate voltage. If the voltage continues to rise beyond a critical limit, an emergency stop mechanism is triggered to protect the system from potential damage.

2.4. Microgrid Software-in-the-Loop Simulation

To fulfill these requirements, the EMS is implemented as a state-based control system using the Stateflow environment in MATLAB/Simulink 2024b. This implementation enables dynamic adjustment of parameters such as bus voltage reference limits or the initial supercapacitor voltage. In this framework, all relevant hardware components—including ESSs and power converters—are modeled within a Simulink simulation. By embedding the control algorithms directly into this environment, developers can verify how effectively the EMS balances energy flows under nominal and extreme conditions (e.g., high and low winds, partial load demands, or transient faults) without endangering physical equipment. Additionally, it allows assessing how much the predictive control component of the EMS can deviate from real conditions while still enabling the feedback control to maintain system stability.

After verifying EMS performance in SiL simulations, its Stateflow code is easily converted into SCL using the Simulink add-on *PLC Coder*, enabling seamless deployment on a PLC. This two-stage process—first refining control logic in a simulated setting, then deploying to real hardware—mitigates risks of malfunction, reduces commissioning time, and ensures fidelity in replication of reel-out/reel-in cycles. Moreover, the SiL approach affords scalability for larger or more complex microgrids and bolsters the potential for future AWES integration by validating the core control principles before on-site implementation.

3. Results

This section presents the results of the proposed EMS implementation and evaluates its performance in managing a ground-generation AWES microgrid within a representative case study. It begins by describing the structure of the control strategy, including the computation of required power and the logic governing transitions between operational phases. The simulation results are then analyzed to demonstrate the EMS's ability to deliver stable power to the grid, regulate bus voltage within acceptable limits, and manage transient power flows under nominal conditions. Finally, initial experimental results obtained from the physical microgrid are analyzed, highlighting the system's adaptability to the highly variable power profile of the AWES.

3.1. EMS Control Strategy Implementation

Figure 6 presents a conceptual state diagram of the proposed EMS control strategy described in subsection 2.2. Prior to energy generation, the system is initialized by energizing the bus to its reference voltage, enabling all power converters, pre-charging the supercapacitor to its initial voltage ($V_{\mathrm{SC}}[0]$), and charging the battery to an acceptable SoC, if it is not already within range.

Between each cycle, the system calculates the power the battery needs to absorb or supply, as defined in Equation 4, and waits for the cycle to start. During the cycle, the supercapacitor's voltage reference ($V_{\mathrm{SC\,ref}}$) and current limit ($I_{\mathrm{SC\,lim}}$) are continuously updated at a high rate to track the rapidly changing AWES power profile.

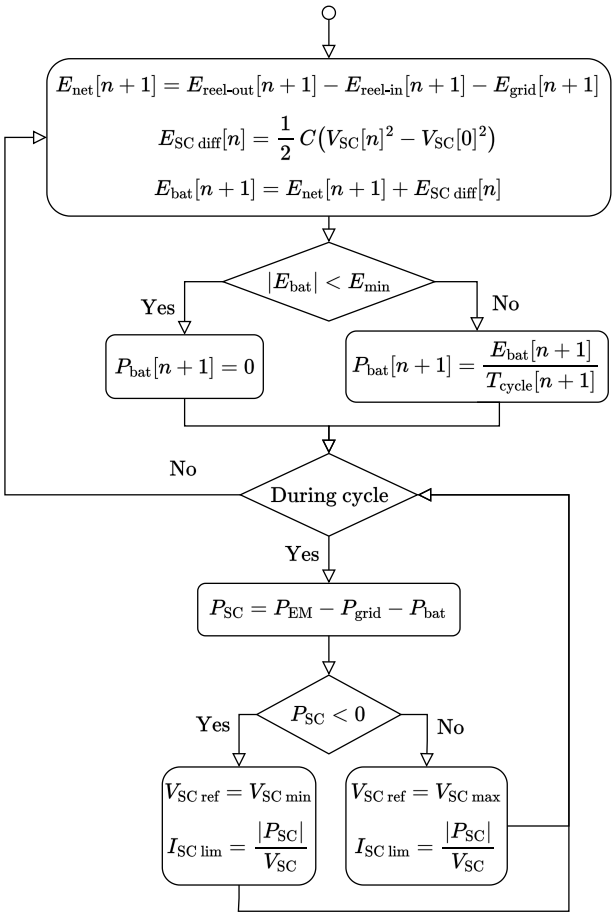

Figure 6: Simplified state diagram of the EMS.

3.2. Simulation Results and Analysis

This subsection presents the results of the SiL simulation for the proposed control strategy under nominal operating conditions of the ground-generation AWES microgrid. It provides a detailed analysis of the EMS operation over two full cycles and demonstrates how this behavior extends across multiple consecutive cycles.

Unlike the simplified profiles shown in Figures 3 and 5, the simulation employs a real AWES power profile obtained from the LAKSA Simulink simulator. Moreover, each cycle exhibits significant variation in generated power, allowing the EMS to be tested under both high- and low-generation scenarios, thereby providing a more realistic representation of real-world operating conditions. Additionally, a normally distributed random variation of $\pm 10\%$ was applied to the net energy term ($E_{\mathrm{net}}[n+1]$) in Equation 3, allowing the EMS to be evaluated under conditions of prediction uncertainty

Figure 7 illustrates the simulated behavior of the system over two full AWES pumping cycles, displaying the bus voltage, key high voltage side currents, and the supercapacitor voltage in p.u.. The nominal value serves as the reference for the bus voltage, the magnitude of the battery's high voltage side current spikes defines the base for system currents, and the supercapacitor's initial voltage is used to scale its own voltage. The figure demonstrates how the supercapacitor charges during the reel-out phase and discharges during the reel-in phase, all while following the current limitation defined in Equation 5 and matching the AWES profile. It also highlights how a constant power flow to the grid is achieved through the proposed energy management strategy.

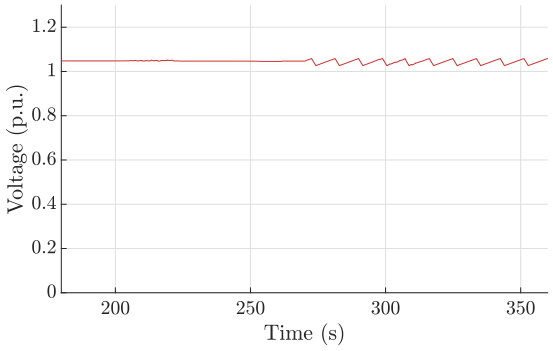

(a) Bus voltage in the simulation.

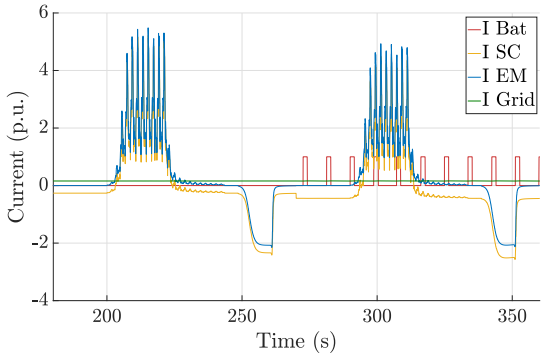

(b) Relevant high voltage side currents of the simulation.

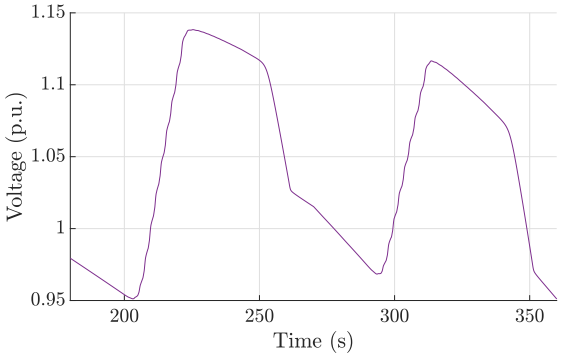

(c) Supercapacitor voltage in the simulation.

Figure 7: Simulation results over two AWES cycles.

During the first cycle, the battery remains idle and the bus voltage is stable. However, after recalculating the required energy for the second cycle using Equation 3, the resulting demand surpasses the minimum threshold (E_{min}), triggering battery participation. Consequently, the superca-

pacitor absorbs less power and delivers more, allowing the bus voltage to rise and enabling the battery to absorb the required energy. The bus voltage during the second cycle creates a sawtooth pattern as mentioned in subsection 2.3.

Figure 8 presents the system's behavior in simulation across multiple pumping cycles. Each cycle's reel-out phase varies in power generation, reflecting differences in wind speed. By contrast, the reel-in phase shows more stable power consumption due to its weaker dependence on wind conditions. The figure illustrates how the proposed EMS effectively maintains the supercapacitor voltage within its defined limits of 0.7–1.3 p.u. by appropriately coordinating battery charging and discharging. Note that the spacing between the battery's current spikes reflects its power demand: higher frequency implies higher demand.

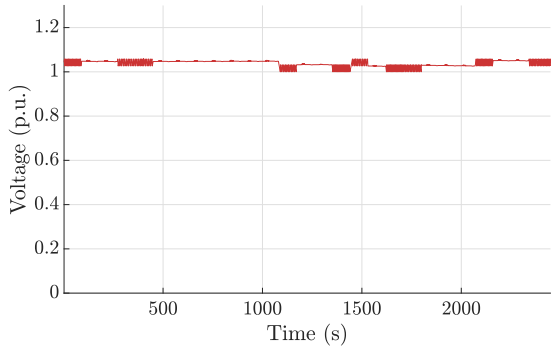

(a) Bus voltage in the simulation.

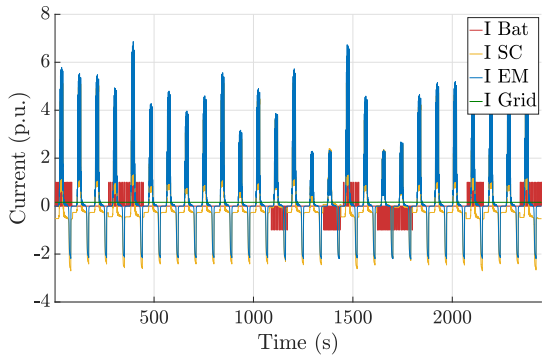

(b) Relevant high voltage side currents of the simulation.

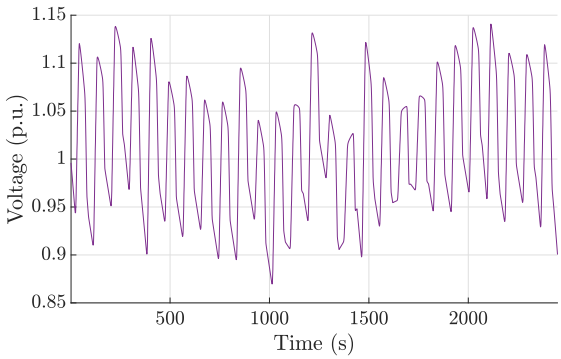

(c) Supercapacitor voltage in the simulation.

Figure 8: Simulation results over many AWES cycles.

These simulation results demonstrate how the supercapacitor effectively mitigates transient power fluctuations, particularly during the reel-out phase, while maintaining bus voltage variations within $\pm 3\%$ of the average value at all times, fluctuating between 1 and 1.06 p.u..

3.3. Experimental Results and Analysis

This subsection presents initial experimental results obtained from the physical microgrid, evaluating the proposed control strategy under nominal operating conditions for the ground-generation AWES system. It includes a detailed analysis of the EMS performance during a single reel-out phase while operating in islanded mode.

Figure 9 illustrates the bus voltage, EM and supercapacitor currents, and the supercapacitor voltage in p.u., using the same reference values defined in subsection 3.2.

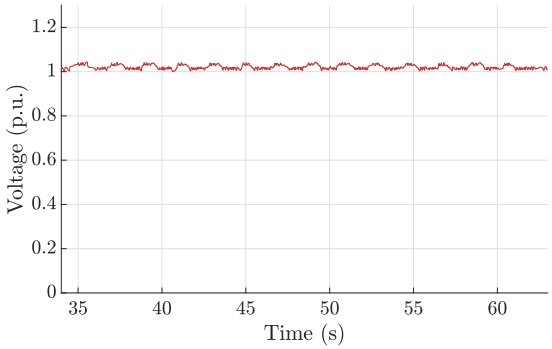

(a) Bus voltage in the microgrid.

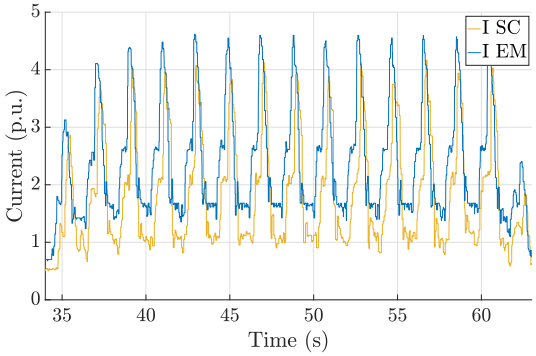

(b) Electric machine and supercapacitor high voltage side currents in the microgrid.

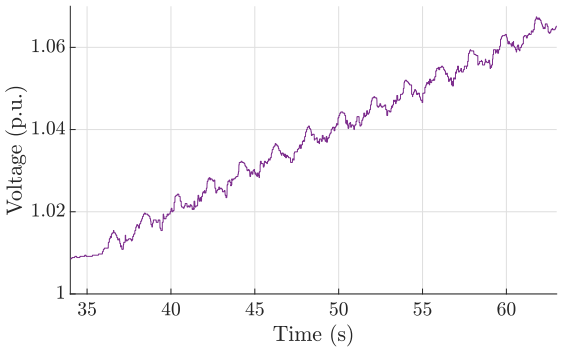

(c) Supercapacitor voltage in the microgrid.

Figure 9: Results over an AWES reel-out.

This initial test demonstrated that the supercapacitor was able to track the highly variable AWES power profile by dynamically adjusting both its voltage reference and current limitation. The offset between the power generated by the EM and the power absorbed by the supercapacitor was greater in the HiL setup than in the SiL simulation, primarily due to communication delays. These delays introduced a slight oscillation in the bus voltage, as shown in Figure 9a, with fluctuations limited to $\pm 1.75\%$, ranging between 1.005 and 1.04 p.u.. This level of oscillation is not

a concern, as it remains within the allowable range for the battery to stay in idle mode.

4. Conclusion

This study underscores the necessity of an EMS for integrating ground-generation AWES into power grids. The cyclical power fluctuations inherent to AWES—with alternating reel-out (high-power generation) and reel-in (energy-consuming) phases—render a direct grid connection unfeasible without advanced control mechanisms. The key findings can be summarized as follows:

- **Critical Role of the EMS**: By dynamically distributing power between energy storage and the grid, the proposed EMS effectively mitigates rapid load changes that would otherwise destabilize grid voltage and frequency.
- **Synergistic Storage Architecture**: Employing a supercapacitor for transient absorption and a battery for longer-term buffering maintains the bus voltage within acceptable deviation limits.
- **Grid Compliance and Reliability**: The control strategy ensures net positive energy export to the grid by managing supercapacitor charging and discharging across reel-out and reel-in phases, thus providing a smoother overall power profile.

Overall, the results confirm that ground-generation AWES technology requires a dedicated EMS to maintain stable operation within typical power grid constraints. The proposed control strategy for the EMS of the AWES power conversion system microgrid in this paper demonstrates its ability to supply constant power to the grid when the only energy source is the power generated by an AWES. The framework presented here offers a scalable foundation for future AWES projects. Future work should focus on expanding HiL testing to validate both the predictive and feedback components of the EMS, as well as its ability to control the battery's power output within the real microgrid.

Acknowledgement

This work is part of the project PID2022-141520OB-I00 funded by MICIU/AEI/ 10.13039/501100011033. This research was funded by CT Ingenieros and Universidad Carlos III de Madrid (UC3M). The author would also like to thank all collaborators who contributed to the development of the simulation platform and control strategies.

References

[1] L. Fagiano and M. Milanese, "Airborne wind energy: An overview," in *2012 American Control Conference (ACC)*. IEEE, 2012, pp. 3132–3143.

[2] A. Cherubini, A. Papini, R. Vertechy, and M. Fontana, "Airborne wind energy systems: A review of the technologies," *Renewable and Sustainable Energy Reviews*, vol. 51, pp. 1461–1476, 2015.

[3] T. Burton, N. Jenkins, E. Bossanyi, D. Sharpe, and M. Graham, *Wind Energy Handbook*, 3rd ed. Hoboken, NJ: Wiley, 2021.

[4] U. Ahrens, M. Diehl, and R. Schmehl, *Airborne Wind Energy*, ser. Green Energy and Technology. Springer, 2013.

[5] P. Bechtle, M. Schelbergen, R. Schmehl, U. Zillmann, and S. Watson, "Airborne wind energy resource analysis," *Renewable Energy*, vol. 141, pp. 1103–1116, 2019.

[6] C. L. Archer and K. Caldeira, "Global assessment of high-altitude wind power," *Energies*, vol. 2, no. 2, pp. 307–319, 2009.

[7] M. Canale, L. Fagiano, and M. Milanese, "High altitude wind energy generation using controlled power kites," *IEEE Transactions on Control Systems Technology*, vol. 18, pp. 279–293, 2010.

[8] M. L. Loyd, "Crosswind kite power," *Journal of Energy*, vol. 4, no. 3, pp. 106–111, 1980.

[9] F. Trevisi, M. Gaunaa, and M. McWilliam, "Unified engineering models for the performance and cost of ground-gen and fly-gen crosswind airborne wind energy systems," *Renewable Energy*, vol. 162, pp. 893–907, 2020.

[10] C. Vermillion and et al., "Electricity in the air: Insights from two decades of advanced control research and experimental flight testing of airborne wind energy systems," *Annual Reviews in Control*, vol. 52, pp. 330–357, 2021.

[11] L. Fagiano, M. Quack, F. Bauer, L. Carnel, and E. Oland, "Autonomous airborne wind energy systems: Accomplishments and challenges," *Annual Review of Control, Robotics, and Autonomous Systems*, vol. 5, 2022.

[12] V. Salma, F. Friedl, and R. Schmehl, "Improving reliability and safety of airborne wind energy systems," *Wind Energy*, vol. 23, no. 2, pp. 340–356, 2020.

[13] U. Fechner, "A methodology for the design of kite-power control systems," Ph.D. dissertation, Technische Universiteit Delft, 2016.

[14] M. S. Ahmed, A. Hably, and S. Bacha, "Kite generator system modeling and grid integration," *IEEE Transactions on Sustainable Energy*, vol. 4, no. 4, pp. 968–976, 2013.

[15] B. Bagaber and A. Mertens, "Energy storage systems for airborne wind generators," in *2022 24th European Conference on Power Electronics and Applications (EPE'22 ECCE Europe)*, 2022, pp. 1–11.

[16] J. Stuyts, K. Geebelen, W. Vandermeulen, J. Driesen, and M. Diehl, "Electrical energy conversion system for an experimental pumping airborne wind energy set-up," 2015-11-20.

[17] R. Mittal, K. Sandhu, and D. Jain, "Battery energy storage system for variable speed driven pmsg for wind energy conversion system," in *2010 Joint International Conference on Power Electronics, Drives and Energy Systems and 2010 Power India*, 2010, pp. 1–5.